Asymmetric shifts in seasonal transition timing in a sub-Arctic river system under climate warming

Abolfazl Jalali Shahrood[1*], Amirhossein Ahrari[1], Ali Torabi Haghighi[1]

[1]Water, Energy and Environmental Engineering Research Unit, University of Oulu, Pentti Kaiterankatu 1, Oulu, P.O.Box 8000, 90570, Finland

[*]*Correspondence to*: Abolfazl Jalali Shahrood (contact@abolfazljalali.com); Present address: Helsinki, Finland (independent researcher).

Abstract. Climate warming is altering the timing of snow and ice processes across northern river systems, yet long-term shifts in their seasonal dynamics remain insufficiently resolved. Here, we analyze a 59-year daily record (1 Oct 1966–30 Sep 2025) from the River Oulankajoki in northeastern Finland to characterize proxy-based seasonal transitions in discharge, snow depth, and air temperature. Using a rule-based detection framework, we identify significant earlier shifts in springtime events, including snow, discharge, and temperature timings. In contrast, autumn/winter timings for those variables exhibit higher year-to-year variability and no consistent trends. Cooling Dominant Period (CDP) and Discharge Stability Period (DSP) have shortened. Over the record the thermal cooling transition shifted progressively later than snow onset, and the thermal warming transition progressively earlier than snow end. This shows that thermal proxies are shifting faster than and progressively diverging from their surface-response counterparts.

1 Introduction

The Arctic's cryo-hydrological systems are experiencing significant changes driven by climate warming. Arctic regions are warming at a rate approximately two to four times faster than the global average, with the most pronounced warming occurring during autumn and winter months (García Criado et al., 2025; Masson-Delmotte et al., 2021; Prowse et al., 2007). Annual average temperatures in the Arctic are expected to rise by approximately 3.7°C by 2050, relative to the 1981–2000 baseline (Prowse et al., 2007). Snow cover extent and duration have generally declined across the Northern Hemisphere in recent decades (Bring et al., 2016), with snow depth and duration projected to continue their downward trends (Burrell et al., 2023). Specifically, Arctic snow cover duration has shortened by approximately 2–4 days per decade over the past 30–40 years, and spring snow cover extent has declined by over 30% since 1971 (Box et al., 2019). Snowmelt is occurring earlier in many regions, often accompanied by more frequent rain-on-snow events (Park et al., 2016). These changes have also affected the timing of spring freshets, which have shifted earlier in Eurasian basins at a rate of about 1.1 days per decade, while North American basins show no significant trends (Feng et al., 2021).

Cryo-hydrological processes in Arctic river systems are experiencing significant transformations driven by climate change. These widespread changes in river flow patterns are primarily driven by rising air temperatures (Pavelsky and Zarnetske, 2017). The timing and magnitude of spring river flows are shifting, with many Arctic rivers transitioning from a nival to a pluvial regime (i.e., snowmelt-dominated to rainfall-dominated) (Prowse et al., 2006). River ice, a critical element of the cryosphere that significantly impacts the global hydrological system, is highly sensitive to weather and hydrological conditions (Shen, 2016). This sensitivity is particularly evident in the Northern Hemisphere, where by 2010, major ice cover existed on 29% of total river lengths, and seasonal ice affected approximately 58% of river lengths (Bennett and Prowse, 2010). Globally, the duration of river ice cover has declined specifically over the past three decades (Newton and Mullan, 2021; Yang et al., 2020), with studies attributing these changes to global warming (Fukś, 2023).

An example is the Danube River, where increasing winter temperatures have reduced its ice cover duration by about 28 days per century (Ionita et al., 2018). Broader analyses using more than 400,000 Landsat images reveal a global average reduction in river ice extent from 10% to 7.5% over the last 30 years (Yang et al., 2020). The most substantial reductions in ice cover duration have occurred in northeastern North America, Central Europe, and areas surrounding the Tibetan Plateau (Fukś, 2023). Ice thickness has also shown widespread decline. For instance, major Arctic rivers in Russia experienced reductions in maximum ice thickness ranging from 2.3 to 12.6 cm per decade between 1955 and 2012 (Fukś, 2023). Numerous studies report overall decreases in river ice thickness across various regions (Nalbant and Sharma, 2023; Vuglinsky, 2017; Vuglinsky and Valatin, 2018).

The timing of river ice freeze-up and break-up has been significantly shifting. Many rivers and lakes around the world exhibit later freeze-up dates and earlier break-up times, which leads to a shorter annual ice cover period (Janowicz, 2010; Newton and Mullan, 2021; Rokaya et al., 2019; Sharma et al., 2022; Shiklomanov and Lammers, 2014; Takács and Kern, 2015; Yang et al., 2020). Long-term records spanning the past 150–200 years provide clear evidence of these trends across Northern Hemisphere lakes and rivers, with freeze-up occurring approximately 5.8 days per century later and break-up about 6.5 days per century earlier (Burrell et al., 2023). On average, ice break-up has moved earlier by about 0.6 days per decade since 1850, correlating with a global temperature increase of about 0.12°C per decade (Fukś, 2023; Magnuson et al., 2000). Freeze-up timing shows greater regional variability, which shows both delayed and earlier occurrences depending on location; however, the dominant global trend is toward later freeze-up dates (Fukś, 2023). Spring and autumn temperatures play critical roles in determining break-up and freeze-up timing, respectively (Brown et al., 2018). Research conducted in the Mackenzie River Delta suggests increasingly earlier spring break-up, with Siberian rivers exhibiting even more pronounced changes than rivers in North America (Podkowa et al., 2023). These shifts are driven primarily by rising springtime air temperatures and indirectly by enhanced river discharge from increased snowmelt (Bieniek et al., 2011; Brown et al., 2018).

Shifts in river ice regimes are disrupting both ecosystems and human activities in the Arctic. Earlier ice break-up and reduced ice cover alter seasonal flooding, nutrient transport, and thermal conditions in aquatic systems, that might affect fish habitats and species composition (Prowse et al., 2006; Yang et al., 2020). These changes also threaten traditional practices, winter transportation, and water resource availability in northern communities (Brown et al., 2018; Fukś, 2023). On land, permafrost thaw is reshaping vegetation, while aquatic ecosystems experience species shifts and declines in fish condition (Lehnherr et al., 2018; Liljedahl et al., 2016).

River ice and cold-climate hydrological processes are important indicators of climate change in Arctic regions, yet their potential is limited by persistent data gaps. River discharge data offer a useful proxy, with the timing and magnitude of spring flows reflecting changes in ice break-up. Increased spring discharge typically accelerates break-up, while autumn and early winter flows influence freeze-up timing (Feng et al., 2021; Park et al., 2016). Among climate variables, air temperature is the dominant driver of ice regimes, strongly correlating with both freeze-up and break-up events (Ionita et al., 2018; Shiklomanov and Lammers, 2014). The freezing index, based on cumulative sub-zero temperatures, is commonly used to estimate ice thickness and seasonal transitions. Specifically, spring temperatures play a critical role in predicting break-up dates (Park et al., 2016). Snow cover is another key proxy, with declining winter snow depths and shorter durations contributing to earlier break-up through reduced surface albedo and enhanced melt (Bring et al., 2016; Lesack et al., 2014). Together, these variables indicate the value of integrating hydrological and climatic data to monitor cryospheric change.

There is a significant shortage of consistent hydrological observations related to river ice across the Arctic, particularly in remote regions (Podkowa et al., 2023). Long-term records of freeze-up and break-up dates, as well as ice thickness, are scarce and often fragmented, that limits the ability to detect robust climate trends (Feng et al., 2021; Park et al., 2016). The decline in river gauging stations since the mid-1980s, especially in Russia and Canada, has further reduced the availability of continuous datasets (Prowse et al., 2007). Inconsistencies in data collection methods and definitions, such as differing criteria for the start or end of ice events, complicate trend analysis and comparisons across regions (Sharma et al., 2022; Yang et al., 2020). For example, some observations record initial break-up, while others note complete ice clearance, a process that may span several weeks (Prowse et al., 2007). These methodological disparities, combined with reduced ground-based monitoring, hinder efforts to separate climate change signals from natural variability and challenge the integration of datasets at the pan-Arctic scale.

Given the persistent data gaps and inconsistencies in direct river ice observations, proxy variables such as air temperature, river discharge, and snow cover have become essential for assessing changes in ice dynamics. These proxies are particularly important in regions where long-term observational records are sparse or incomplete. In response to this challenge, the present study builds on the River Ice Timing Characteristics and Extremes (RiTiCE) framework developed in MATLAB (Jalali Shahrood et al., 2023) to characterize long-term proxy-based transition timing in the River Oulankajoki in northern Finland. RiTiCE is a rule-based framework that detects Phase Change Timings (PCTs) from daily discharge, snow depth, and air temperature time series. From these PCTs, Intra-Variable Intervals (IVIs) and Cross-Variable Intervals (CVIs) are derived to describe timing relationships between thermally-derived (i.e., air temperature) and surface response (i.e., discharge and snow depth) transitions. In this study, PCTs are grouped into an *onset-group* (autumn/winter transitions) and a *release-group* (spring transitions). RiTiCE has been validated across multiple Arctic and sub-Arctic river systems, including the Tornionjoki, Kiiminkijoki, Kemijoki, and Tana rivers (Jalali Shahrood, 2023; Jalali Shahrood et al., 2024). This study aims to answer the following research questions:

(1) How have the PCTs shifted over the observational record?

(2) How have the derived IVIs and CVIs changed, and do these changes differ between the onset-group and the release-group?

(3) How has the temporal coupling between thermally-derived PCTs and their surface response evolved in terms of the direction and magnitude of cross-variable timing offsets?

2 Methodology

2.1 Phase Change Timings (PCTs)

RiTiCE is applied to annual daily time series of discharge, snow depth, and air temperature to detect transition timings in each variable. Input data must be prepared under consistent preprocessing rules and analyzed using variable-specific transition detection methods.

The datasets must be prepared as follows:

- Leap days (29 February) must be removed to maintain a uniform 365-day structure across all years.
- Data must be reorganized by Water Year (WY), defined from October 1st to September 30th.

RiTiCE detects PCTs, IVIs, and CVIs from annual daily time series of discharge, snow depth, and air temperature. The timings may not necessarily correspond directly to observed processes such as ice formation, break-up, or snowmelt but were earlier tested against recorded ice condition data in previous studies (Jalali Shahrood et al., 2023, 2024). The timings at which a variable undergoes detected transition are referred to as PCTs and defined in Table 1.

From PCTs, two types of derived metrics are constructed: (i) IVIs which describe durations between PCTs within a single variable, and (ii) CVIs, which quantify signed timing offsets between two PCT dates from different variables. IVIs and CVIs are summarized in Tables S1–S2. We report only the primary IVIs defined between each variable's PCTs; their complementary intervals are deterministic 365-day complements and therefore redundant.

Table 1 Summary of PCTs detected by RiTiCE, their definitions, variables used and methods applied. Legacy labels (e.g., FUD, BUD, SBD, SMD, TTP−/TTP+) are omitted to avoid misinterpretation of PCTs as direct representations of freeze-up, break-up, or snowmelt events.

PCT	**Legacy PCT**	**Definition**	**Variable**	**Method**
DSO (Discharge Stabilization Onset)	FUD	Start of the longest period of reduced discharge variability	Discharge	DVD (Daily Value Difference)
DSE (Discharge Stabilization End)	BUD	End of the longest period of reduced discharge variability	Discharge	DVD (Daily Value Difference)
CSO (Continuous Snow Onset)	SBD	Start of the longest continuous period of non-zero snow depth	Snow depth	LSS (Longest Snow Sequence)
CSE (Continuous Snow End)	SMD	End of the longest continuous period of non-zero snow depth	Snow depth	LSS (Longest Snow Sequence)
CCT (Cumulative Cooling Transition)	TTP$^-$	Transition to cumulative cooling dominance	Temperature	ZCAT (Zero-Referenced Cumulative Area Transition)
CWT (Cumulative Warming Transition)	TTP$^+$	Transition to cumulative warming dominance	Temperature	ZCAT (Zero-Referenced Cumulative Area Transition)

Figure 1 summarizes how RiTiCE detects PCTs and IVIs from daily time series. Three variables of discharge, snow depth, and air temperature are processed using variable-specific methods. The DVD method detects Discharge Stabilization Onset and End (DSO, DSE), LSS identifies Continuous Snow Onset and End (CSO, CSE), and ZCAT defines Cooling and Warming Transitions (CCT, CWT). Each PCT pair defines an IVI, Discharge Stability Period (DSP: DSO–DSE), Continuous Snow Period (CSP: CSO–CSE), and Cooling Dominant Period (CDP: CCT–CWT).

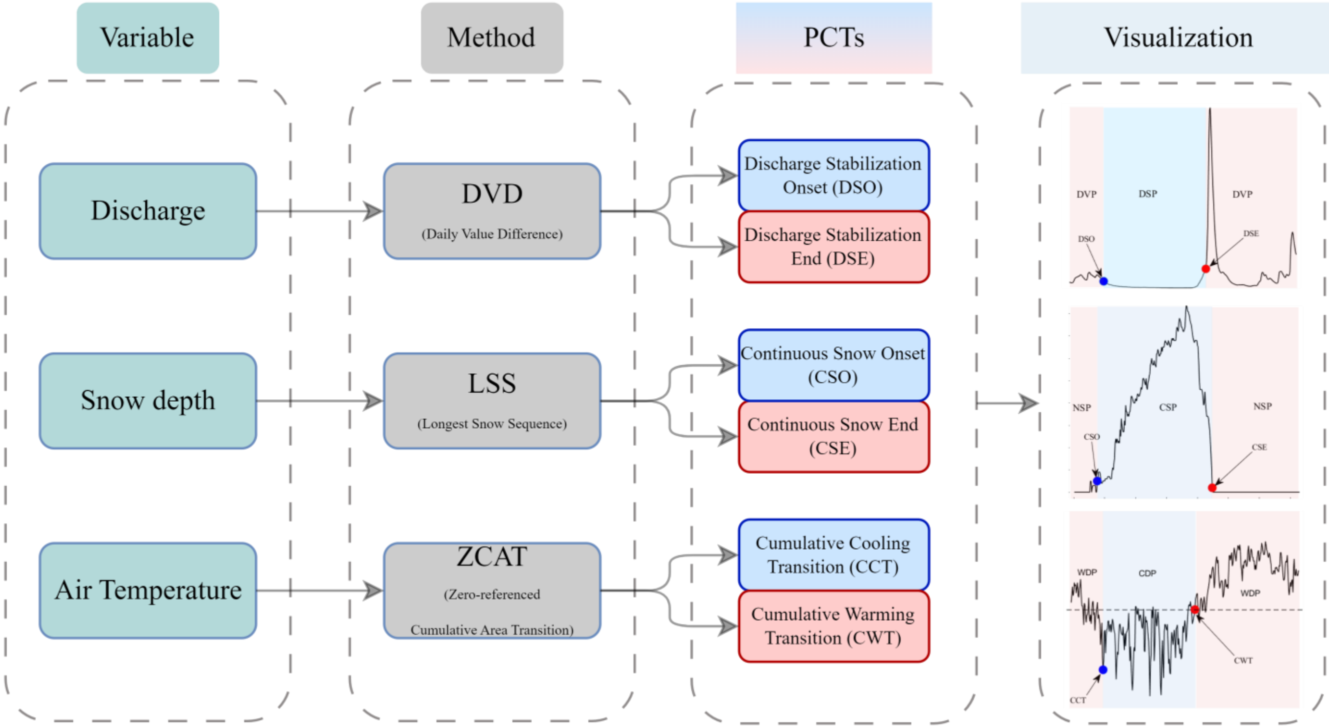

Figure 1 Overview of the PCT (Phase Change Timing) feature extraction framework.

2.2 Discharge Phase Change Timings (PCTs): Discharge Stabilization Onset and End (DSO & DSE)

In RiTiCE, DSO and DSE represent transition timings inferred from changes in discharge variability rather than direct observations of river ice conditions. DSO and DSE capture changes in discharge variability that may be associated with ice-related processes, but are not equivalent to visually observed freeze-up or break-up dates as defined by the International Association for Hydraulic Research (IAHR, 1980); although they can be compared with as reported in earlier studies (Jalali Shahrood et al., 2023, 2024).

Discharge stabilization is detected using the Daily Value Difference (DVD) method. Daily changes in discharge were computed between consecutive days as forward differences:

$$\Delta Q_t = Q_{t+1} - Q_t \quad (1)$$

Note. An equivalent backward-difference definition $\Delta Q_t = Q_t - Q_{t-1}$ uses the same consecutive-day differences with a one-day index shift and therefore yields the same stability structure; detected DSO/DSE are not materially sensitive to this choice.

For each WY (365 days), this yields $N = 364$ day-to-day changes in discharge ΔQ_t. Variability of ΔQ_t across the entire WY is summarized by:

$$\sigma_{\Delta Q} = \sqrt{\frac{1}{N}\sum_{t=1}^{N}\left(\Delta Q_t - \overline{\Delta Q}\right)^2}, \quad (2)$$

We classify day-to-day changes as stable when $|\Delta Q_t| \leq \sigma_{\Delta Q}$. DSE is taken as the day of WY corresponding to the end of the longest contiguous sequence of stable daily changes in the full WY, with day indices obtained by applying a consistent one-day offset to the ΔQ_t series.

In a second step, discharge and day-to-day changes are restricted to the period before DSE, a separate variability threshold is computed from those pre-DSE day-to-day changes only, and DSO is taken as the start of the longest contiguous stable segment under that pre-DSE threshold (with one-day offset). A pre-DSE threshold is used because day-to-day change differs across hydrograph phases, and DSO is constrained to occur before DSE. DSP is then defined as the interval between DSO and DSE (DSP = DSE − DSO) (Figure 2).

$$\mathrm{DSE} = max\{t_k\} + 1 \quad \text{where} \quad \left|\Delta Q_{t_k}\right| \leq \sigma_{\Delta Q} \quad (3)$$

$$\mathrm{DSO} = min\{s_k\} + 1 \quad \text{where} \quad \left|\Delta Q_{s_k}\right| \leq \sigma_{\Delta Q}^{\mathrm{pre}} \quad (4)$$

Where:

Q_t: discharge on day t (m^3/s)

ΔQ_t: day-to-day change $Q_{t+1} - Q_t$ (m^3/s)

$N = 364$: number of day-to-day changes in a 365-day WY

$\overline{\Delta Q}$: mean of ΔQ_t over the WY

t_k = indices of the longest contiguous run in the full WY with $|\Delta Q_t| \leq \sigma_{\Delta Q}$

s_k = indices of the longest contiguous run before DSE with $|\Delta Q_t| \leq \sigma_{\Delta Q}^{\mathrm{pre}}$

$\sigma_{\Delta Q}$: standard deviation of ΔQ_t over the full WY (used for DSE)

$\sigma_{\Delta Q}^{\mathrm{pre}}$: standard deviation of ΔQ_t computed on day-to-day changes before DSE (used for DSO)

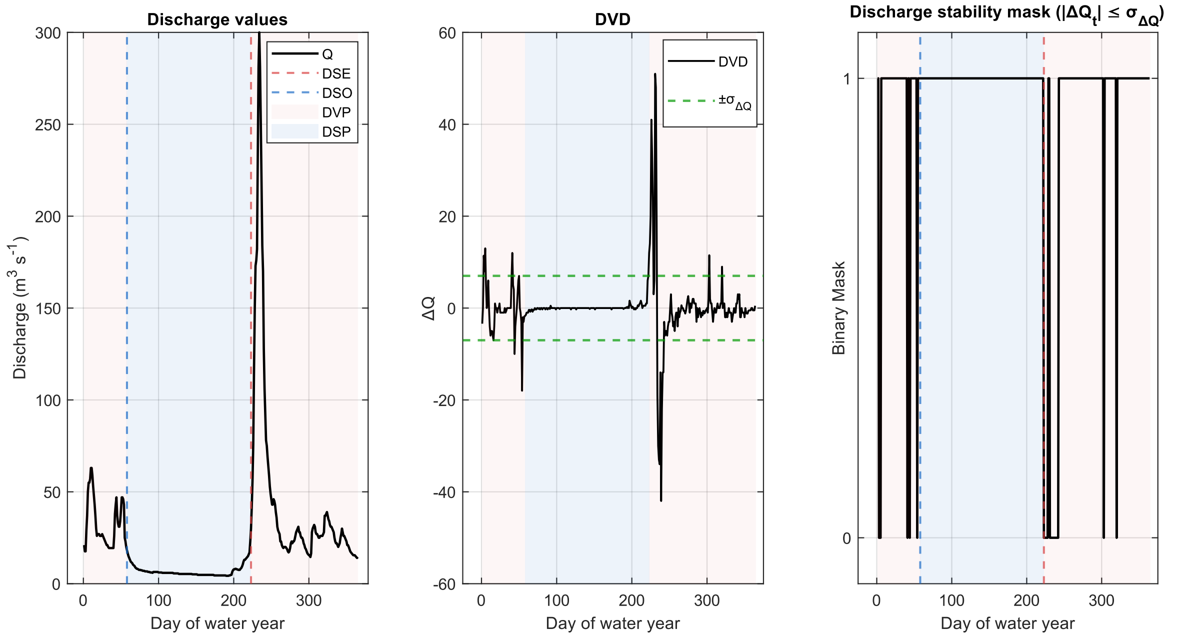

Figure 2 Detection of Discharge Stabilization Onset (DSO) and Discharge Stabilization End (DSE) using discharge data. (Left) Daily discharge with DSO (blue dashed line) and DSE (red dashed line). (Center) Daily Value Difference (DVD) showing day-to-day changes in discharge. (Right) Binary discharge stability mask derived from $|\Delta Q_t| \le \sigma_{\Delta Q}$. Each day-to-day change $\Delta Q_t = Q_{t+1} - Q_t$ is classified as stable (mask = 1) if $|\Delta Q_t| \le \sigma_{\Delta Q}$, otherwise unstable (mask = 0).

2.3 Snow Depth Phase Change Timings (PCTs): Continuous Snow Onset and End (CSO & CSE)

To determine the timing of persistent snow cover, we apply the Longest Snow Sequence (LSS) method (Figure 3). A binary snow presence mask is generated from daily snow depth values, where each day is assigned a value of 1 if snow is present (S ≠ 0) and 0 otherwise:

$$M_t = H(S_t), \quad \text{where } H(x) = \begin{cases} 1, & x > 0 \\ 0, & x = 0 \end{cases} \tag{5}$$

LSS identifies the longest M_t=1 segment and hence CSO and CSE; CSP is then the period between CSO and CSE:

$$[\text{CSO} = t_{\text{start}}, \quad \text{CSE} = t_{\text{end}}] \qquad M_t = 1 \quad \forall\, t \in [t_{\text{start}}, t_{\text{end}}] \tag{6}$$

Where:

S_t = Snow depth on day t (in cm), for t ∈ {1, 2, ..., 365}

M_t = Binary snow presence mask

$[t_{start}, t_{end}]$ = Indices of the longest continuous subsequence such that $M_t = 1$ for all $t \in [t_{start}, t_{end}]$

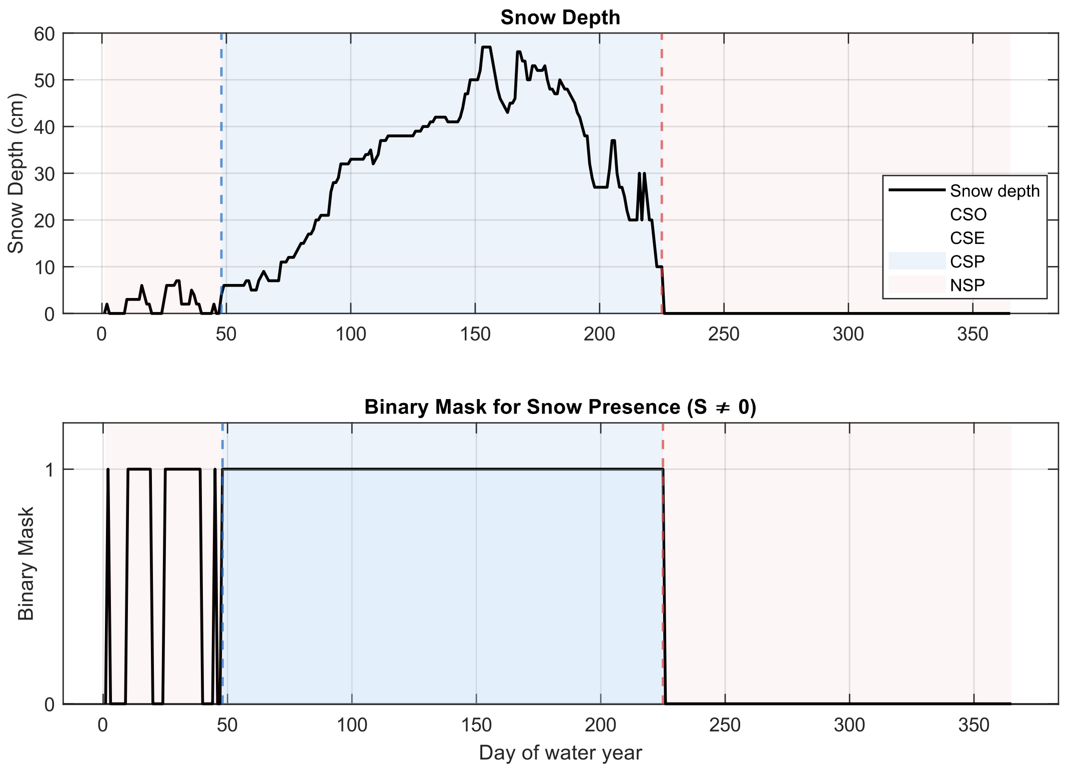

Figure 3 Detection of Continuous Snow Onset (CSO) and Continuous Snow End (CSE) from snow depth data. (Top) Daily snow depth with CSO (blue dashed line) and CSE (red dashed line). (Bottom) Binary snow presence mask used to identify the longest Continuous Snow Period (CSP).

2.4 Air Temperature Phase Change Timings (PCTs): Cumulative Cooling and Warming Transitions (CCT & CWT)

Temperature transitions are characterized using the Zero-Referenced Cumulative Area Transition (ZCAT) method, which captures the integrated thermal state by accumulating daily areas between the temperature curve and the 0 °C baseline (Figure 4). ZCAT is used because it returns a single within-year transition date for each of the cooling and warming phases directly from the cumulative curve. Freezing and thawing degree-day sums (FDD and TDD) quantify accumulated thermal energy in °C days but do not by themselves define a transition date without an additional threshold or breakpoint rule. FDD and TDD are therefore reported separately as complementary thermal context (Section 3.4) rather than as timing definitions. For each day t, the area between day t and t + 1 is computed using the trapezoidal rule:

$$A_t = \frac{T_t + T_{t+1}}{2} \quad (7)$$

The cumulative temperature area is then given by:

$$C_t = \sum_{i=1}^{t} A_i \quad (8)$$

where:

- T_t= daily mean temperature on day t
- A_t = area contribution between day t and $t + 1$
- C_t = Cumulative curve
- CCT = the last zero-crossing of C_t prior to CWT, marking the transition from cumulative warming to cumulative cooling dominance.
- CWT = the day at which C_t reaches its minimum, marking the transition from cumulative cooling to cumulative warming dominance.

Note. In one water year (WY2009), C_t did not cross zero within the water-year window, and CCT defaulted to the first day of the water year. Inspection of the preceding water year showed that the corresponding zero-crossing fell at the end of September, just before the water-year boundary. Because this affects a single year, the water-year definition and the ZCAT procedure are kept unchanged.

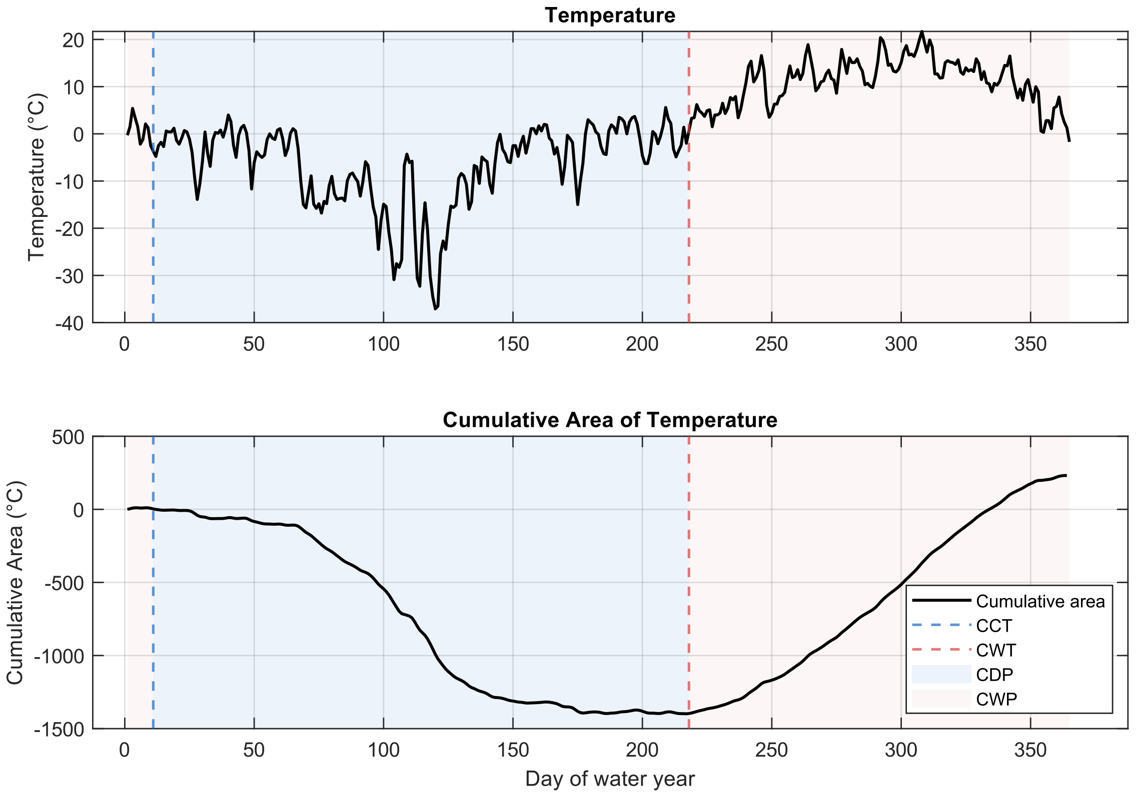

Figure 4 Detection of Cumulative Cooling Transition (CCT) and Cumulative Warming Transition (CWT) using Zero-Referenced Cumulative Area Transition (ZCAT). (Top) Daily air temperature. (Bottom) Cumulative temperature curve, used to detect CCT & CWT. As A_t is computed between t and $t+1$, reported transition days follow the same $+1$ index mapping.

2.5 Data

Daily air temperature and snow depth records were obtained from the Finnish Meteorological Institute (FMI) Open Data Portal (Finnish Meteorological Institute, 2026), specifically from the Kuusamo Kiutaköngäs weather station (N66°22'4", E29°19'40"), about 500 meters away from the Oulanka Research Station. These records span from October 1966 to September 2025 (WY1966–WY2024). Snow depth is recorded in whole centimetres; the FMI code −1 (trace) was recoded to 0 (no snow) prior to analysis. A total of 12 missing non-consecutive days across the 59-year record were interpolated to maintain a complete daily series. The observational accuracy for snow depth is ±2 cm. Daily river discharge measurements were acquired from the Oulanka Research Station (daily mean), hosted by the Finnish Environment Institute (SYKE, 2026). Winter discharge values in the Hertta database are flagged as 'Redukoitu' (quality code '='), meaning they are estimates derived from post-processing corrections applied when ice conditions affect the rating curve relationship. The DVD-based proxies (DSO, DSE) are therefore derived from a quality-controlled rather than a directly measured record, and DSO/DSE should be interpreted as discharge regime transition proxies rather than direct ice phenology dates.

In addition to discharge, snow depth, and air temperature used for RiTiCE, we analyzed ancillary datasets of water temperature and ice thickness (available for limited periods). These records are operationally constrained (e.g., seasonal deployment, access/safety, and quality control) and therefore are not treated as direct freeze-up/break-up observations. Instead, they are used as contextual support to assess whether the PCTs occur in a plausible seasonal neighborhood to these operations (Figure S2). The ancillary datasets were obtained from SYKE open data platform (SYKE, 2026).

2.6 Trends and correlations analysis

Long-term monotonic trends in annual PCT, IVI, and CVI series, and in the hydroclimatic extremes, were tested using the Mann–Kendall test (Kendall, 1975; Mann, 1945). To reduce potential inflation of significance arising from serial autocorrelation, each series was pre-whitened by removing the AR(1) component prior to testing (Von Storch, 1999). This pre-whitened Mann–Kendall procedure is referred to as PW-MK throughout results. Statistical significance was evaluated at $p < 0.05$. Trend magnitude was quantified using Sen's slope (Sen, 1968), reported in the native units of each metric (days yr^{-1} for PCTs and IVIs; signed days yr^{-1} for CVIs).

Associations among PCTs and IVIs over the full record were assessed using Spearman rank correlations (ρ) (Spearman, 1904), computed on paired water-year values. Correlation p-values are reported alongside ρ. The record was also divided into an early period (WY1966–WY1994) and a late period (WY1995–WY2024) to evaluate changes in timing structure between the two halves of the study period.

2.7 Study Area

River Oulankajoki (Figure 5) is a boreal river system located in northeastern Finland near the Arctic Circle (Arvola and Nurmesniemi, 2000; Saraniemi et al., 2008). Situated within the boreal zone, it displays cold-climate hydrological characteristics, including seasonal snow accumulation, extended ice cover, and distinct freeze-thaw cycles. Hydrologically, the river is strongly seasonal (Blåfield et al., 2024; Saraniemi et al., 2008). The mean annual discharge is approximately 25.5 m^3/s, with low flows dropping to around 3 m^3/s in late winter and peak flows reaching up to 249 m^3/s during the spring snowmelt in May–June. The river typically freezes from mid-November to early May. Recent climatic trends show significant warming in the region, with average temperatures rising by 0.61°C per decade and summer temperatures by 0.41°C per decade. These trends are shortening the winter season and altering the basin's overall hydroclimatic regime. Over the past five decades, spring floods have weakened by 7%, while high-flow events in other seasons have increased by 10%. Annual minimum flows have risen by 28%, that reflects both climatic and hydrological shifts (Blåfield et al., 2024).

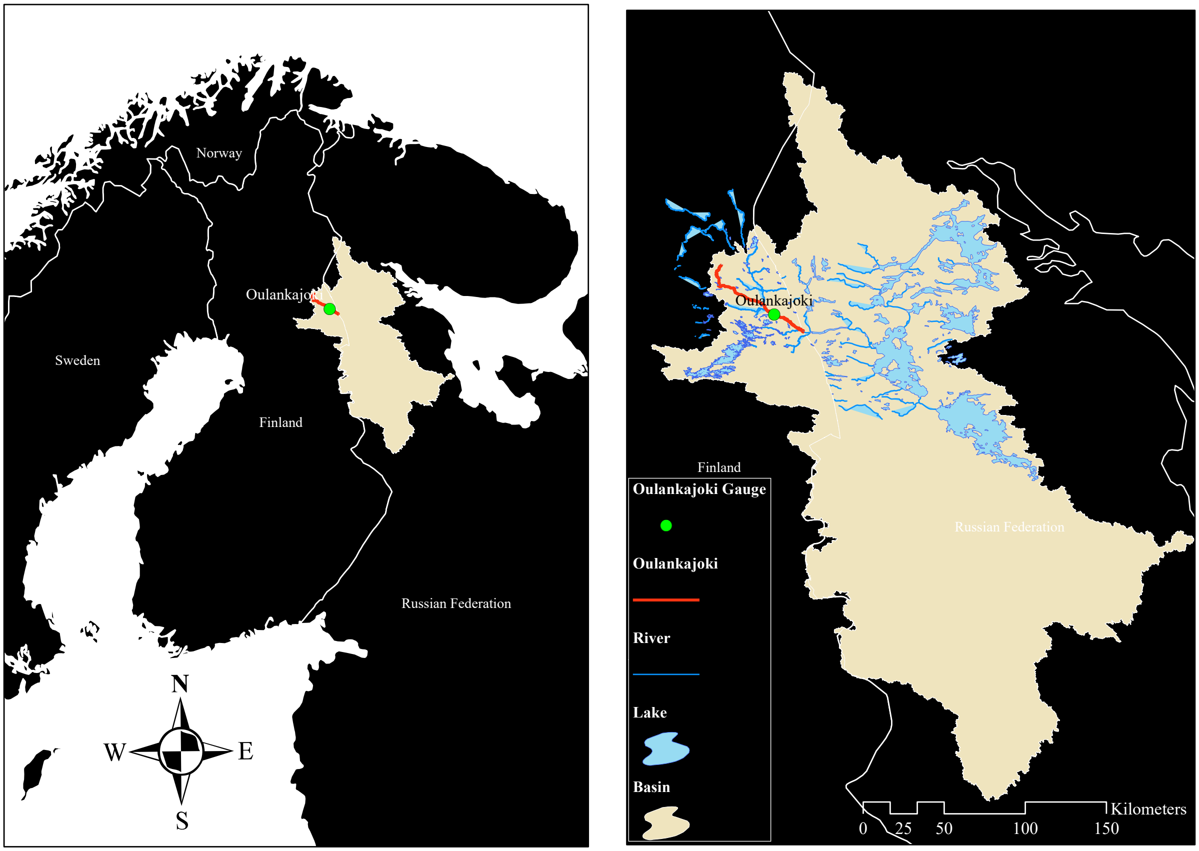

Figure 5 Location of the River Oulankajoki basin.

3 Results

3.1 Distribution and Early–Late Shifts of PCTs

Over the 59-year record (WY1966–WY2024, n=59), the six PCTs ranged across distinct portions of the WY (Figure 6; embedded table). Among the onset-group, DSO ranged from day 15 to day 95 (median 49, SD ±17.5 d). CSO ranged from day 5 to day 70 (median 34, SD ±14.4 d). CCT ranged from day 1 to day 88 (median 38, SD ±20.9 d; the day 1 value corresponds to WY2009, see Section 2.4). Among the release-group, DSE ranged from day 196 to day 231 (median 216, SD ±8.6 d). CSE ranged from day 206 to day 238 (median 224, SD ±7.0 d). CWT ranged from day 177 to day 222 (median 201, SD ±10.9 d). CCT showed the largest spread and CSE showed the smallest of all six PCTs.

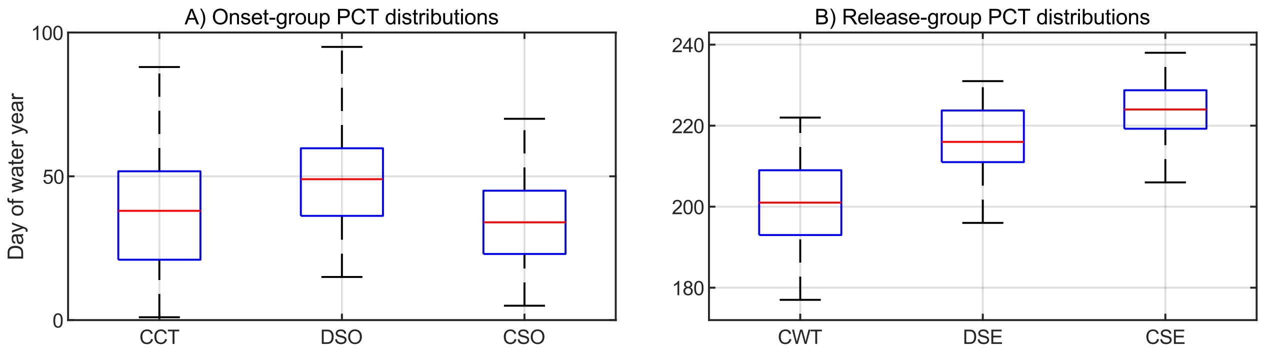

PCT	Mean ± SD	Median [p10–p90]	Min	Max
DSO	50.0 ± 17.5	49 [27–72]	15	95
DSE	216.3 ± 8.6	216 [205–226]	196	231
CSO	34.6 ± 14.4	34 [19–51]	5	70
CSE	223.5 ± 7.0	224 [214–233]	206	238
CCT	38.0 ± 20.9	38 [12–66]	1	88
CWT	200.3 ± 10.9	201 [184–214]	177	222

Figure 6 Summary of PCTs over 59 years.

The record was divided into two approximately equal sub-periods to allow balanced comparison of early and late period distributions. Comparing the early period (WY1966–WY1994, n=29) with the late period (WY1995–WY2024, n=30), all three onset-group PCTs shifted to later days of the WY (Figure 7). DSO shifted by +2.5 d (median: day 48.0 to day 50.5). CSO shifted by +4.0 d (median: day 34.0 to day 38.0). CCT shifted by +17.5 d (median: day 30.0 to day 47.5). All three release-group PCTs shifted to earlier days of the WY. DSE shifted by −3.0 d (median: day 218.0 to day 215.0). CSE shifted by −1.5 d (median: day 224.0 to day 222.5). CWT shifted by −12.5 d (median: day 208.0 to day 195.5). Decadal-binned distributions of all six PCTs across consecutive 10-year blocks (WY1966–WY1975 through WY2016–WY2024) are provided in Supplementary Figure S1; in the decadal-binned distributions, CCT and CWT showed the most consistent directional progression across successive decades, while DSO, CSO, DSE, and CSE varied across decadal blocks without a monotonic step pattern.

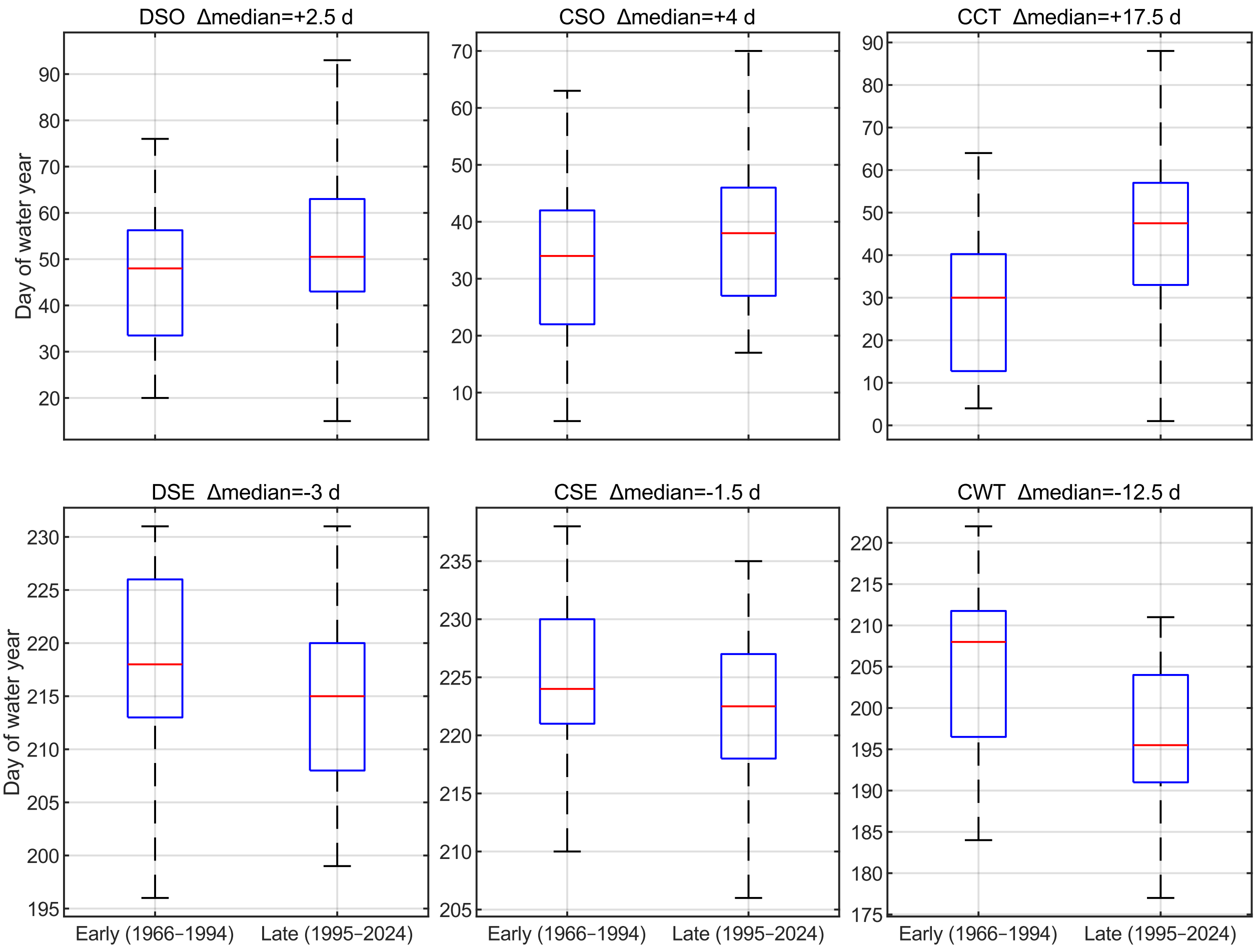

Figure 7 Early vs late period distributions of PCTs (day of WY) for WY1966–WY1994 (n=29) and WY1995–WY2024 (n=30); panel titles report the change in median timing (late − early, days). Top row shows onset-group PCTs and bottom row release-group PCTs. Left column shows discharge PCTs, middle snow depth PCTs, and right air temperature PCTs.

3.2 Ordering Patterns and Interannual Variability of PCT Sequencing

The onset-group varied in ordering across the full record (WY1966–WY2024, n=59; Figure 8A). Five of the six possible orderings occurred at least once. The most frequent ordering was CSO→CCT→DSO, occurring in 25 years (42.4%). CCT→CSO→DSO occurred in 13 years (22.0%), CSO→DSO→CCT in 11 years (18.6%), CCT→DSO→CSO in 7 years (11.9%), and DSO→CSO→CCT in 3 years (5.1%). The ordering DSO→CCT→CSO did not occur in any year. Across the full record, DSO preceded CCT in 14 of 59 years (23.7%), and DSO preceded CSO in 7 of 59 years (11.9%). Three water years illustrate how these reversals arise (Figure S3). In WY1975, a short early snow spell fell outside the longest continuous snow segment, so CSO was set later and the order was CCT, DSO, CSO. In WY2011, discharge stabilized while the cumulative cooling transition was delayed, giving the order CSO, DSO, CCT. In WY2020, discharge stabilized early and the initial snow record again fell outside the continuous segment, giving the order DSO, CSO, CCT. The release group occupied a fixed global ordering in all 59 years: CWT→DSE→CSE occurred in 100% of WYs (Figure 8B). DSO, CSO, and CCT each ranged across global ranks 1, 2, and 3, with no PCT holding a fixed rank position in any year, while CWT held global rank 4, DSE rank 5, and CSE rank 6 in every year (Figure 8G).

Comparing the early (WY1966–WY1994, n=29; Figures 8C–D) and late (WY1995–WY2024, n=30; Figures 8E–F) sub-periods, the release-group invariance (CWT→DSE→CSE, 100%) held in both periods without exception. Within the onset group, the ordering CSO→CCT→DSO was the most frequent in both periods (37.9% early, tied with CCT→CSO→DSO at 37.9%; 46.7% late).

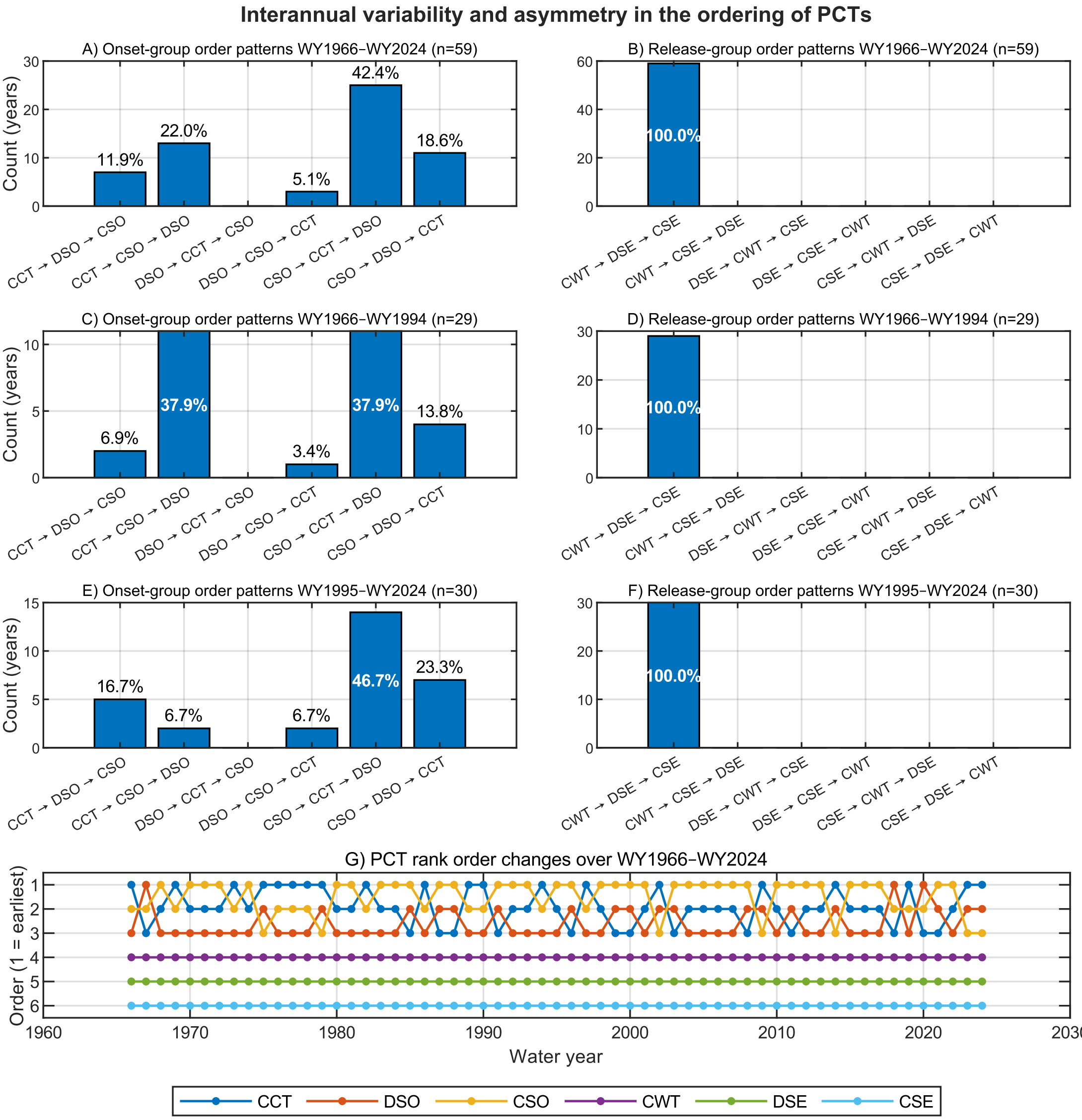

325 **Figure 8 Interannual variability and asymmetry in the ordering of PCTs (WY1966–WY2024, n=59). (A) Onset-group ordering frequencies, full record. (B) Release-group order-pattern frequencies, full record. (C) Onset-group order-pattern frequencies, early period (WY1966–WY1994, n=29). (D) Release-group ordering frequencies, early period. (E) Onset-group ordering frequencies, late period (WY1995–WY2024, n=30). (F) Release-group ordering frequencies, late period. (G) Year-to-year PCT rank order changes across the full record (rank 1 = earliest in that water year).**

3.3 Spearman Correlations Among PCTs and IVIs - Full Record and Early-Late Comparison

Within the release-group, DSE and CSE showed the strongest PCT correlation ($r=0.74$, $p<0.001$), followed by DSE and CWT ($r=0.60$, $p<0.001$) and CSE and CWT ($r=0.53$, $p<0.001$) over the 59-year record. Within the onset-group, DSO and CSO ($r=0.46$, $p<0.001$), DSO and CCT ($r=0.48$, $p<0.001$), and CSO and CCT ($r=0.49$, $p<0.001$) were all significant and positive (Figure 9A).

In the early period (WY1966–WY1994, $n = 29$), the strongest correlations were DSE and CSE ($r = 0.82$, $p < 0.001$) and DSE and CWT ($r = 0.67$, $p < 0.001$). DSO and CSO ($r = 0.64$, $p < 0.001$) and CSE and CWT ($r = 0.55$, $p = 0.002$) were also significant (Figure 9B).

In the late period (WY1995–WY2024, $n = 30$), DSO and CCT, and CSO and CCT, increased to $r = 0.52$ ($p = 0.003$) and $r = 0.68$ ($p < 0.001$), respectively, while DSE and CSE, DSE and CWT, and CSE and CWT, decreased to $r = 0.60$ ($p < 0.001$), $r = 0.44$ ($p = 0.015$), and $r = 0.44$ ($p = 0.016$), respectively. DSO and DSE showed a significant negative correlation ($r=-0.45$, $p=0.013$) in the late period (Figure 9C).

For IVIs over the full record, all three pairings were significant and positive: DSP and CSP ($r=0.55$, $p<0.001$), DSP and CDP ($r=0.57$, $p<0.001$), and CSP and CDP ($r=0.58$, $p<0.001$) (Figure 9D). In the early period, DSP and CSP ($r=0.61$, $p<0.001$) and DSP and CDP ($r=0.43$, $p=0.021$) were significant; CSP and CDP did not reach significance ($r=0.36$, $p=0.052$) (Figure 9E). In the late period, DSP and CSP ($r=0.39$, $p=0.033$), DSP and CDP ($r=0.54$, $p=0.002$), and CSP and CDP ($r=0.69$, $p<0.001$) were all significant (Figure 9F), with CSP and CDP showing the strongest IVI correlation of either period.

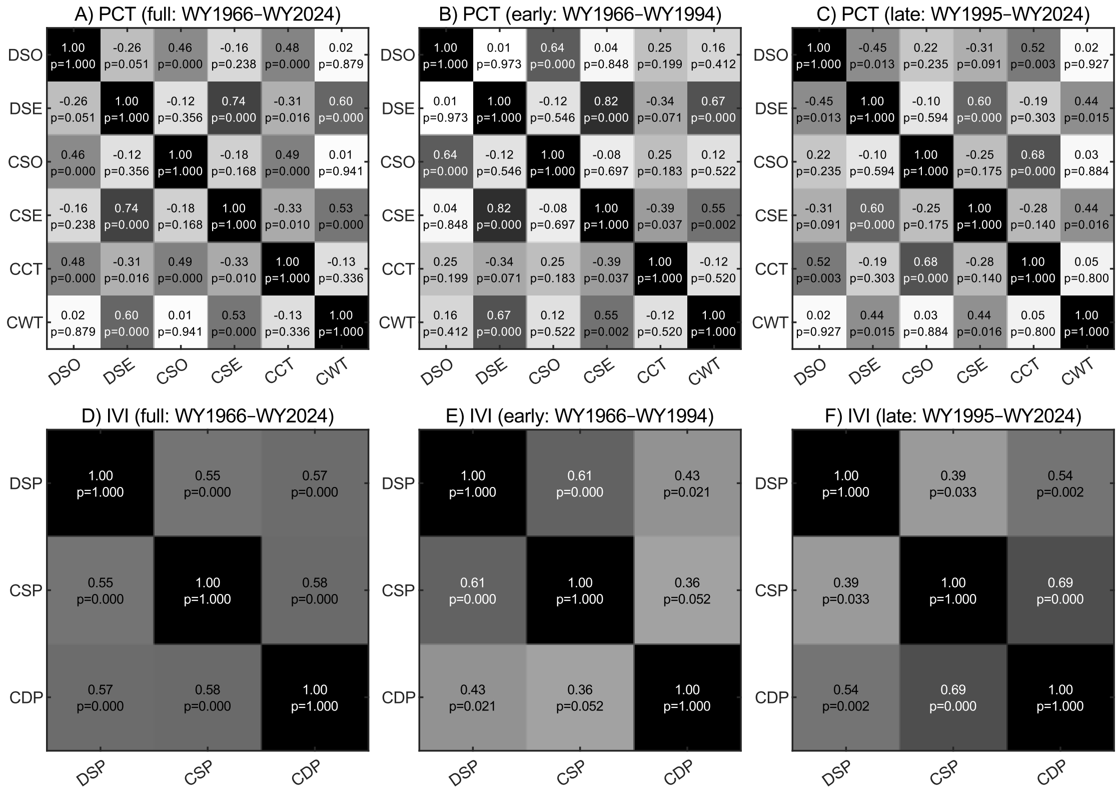

Figure 9 Spearman correlation matrices for PCTs (top row, panels A–C) and IVIs (bottom row, panels D–F) for the full record (WY1966–WY2024, n=59), early period (WY1966–WY1994, n=29), and late period (WY1995–WY2024, n=30).

3.4 Long-term Trends in PCT, IVI, CVI, Temperature, Freeze–Thaw Degree-Days, and Hydroclimatic Extremes

Among the six PCTs, CCT shifted later at +0.538 d/yr (PW-MK p=0.001) and CWT shifted earlier at −0.357 d/yr (p=0.002). DSE shifted earlier at −0.182 d/yr (p=0.023) and CSE at −0.118 d/yr (p=0.038). DSO (Sen=+0.154 d/yr, p=0.281) and CSO (Sen=+0.128 d/yr, p=0.252) showed no significant trend. Among the IVIs, CDP decreased at −0.871 d/yr (p<0.001) and DSP decreased at −0.333 d/yr (p=0.041). CSP showed a negative Sen slope (−0.233 d/yr) but did not reach significance (p=0.089) (Figure 10).

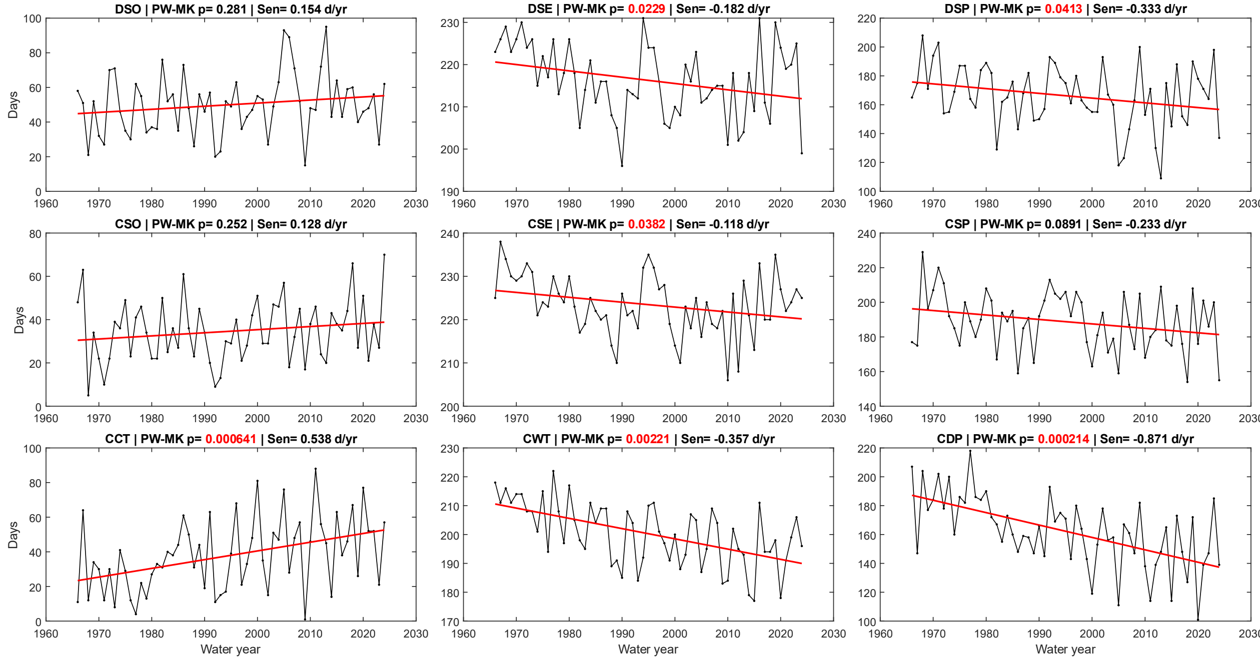

Figure 10 Long-term trends in Phase Change Timings (PCTs) and Intra-Variable Intervals (IVIs) (WY1966–WY2024; n=59). Significant p-values are highlighted in red.

365 The offset between CSE and CWT decreased at −0.231 d/yr (p=0.011), and the offset between CSO and CCT increased at +0.333 d/yr (p=0.040). The remaining four CVIs showed no significant trend, the offset between DSO and CSO (Sen=+0.074 d/yr, p=0.505), between DSO and CCT (Sen=+0.222 d/yr, p=0.103), between DSE and CSE (Sen=0.000 d/yr, p=0.958), and between DSE and CWT (Sen=−0.167 d/yr, p=0.102) (Figure 11).

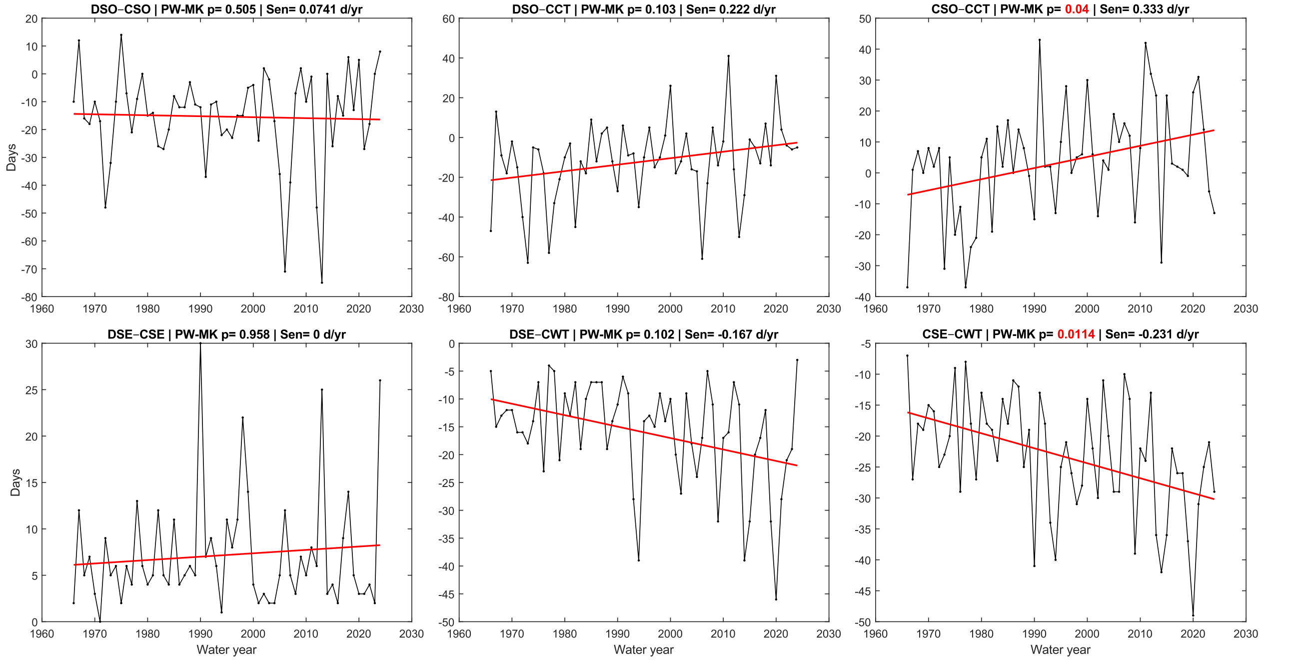

Figure 11 Long-term trends in cross-variable timing offsets (CVIs) derived from PCT pairs (WY1966–WY2024; n=59).

Mean air temperature increased significantly in all three seasonal windows (Figure 12), with Oct–Dec at +0.066 °C/yr (p=0.001), Mar–May at +0.037 °C/yr (p=0.008), and the Nov–Apr window at +0.067 °C/yr (p=0.004).

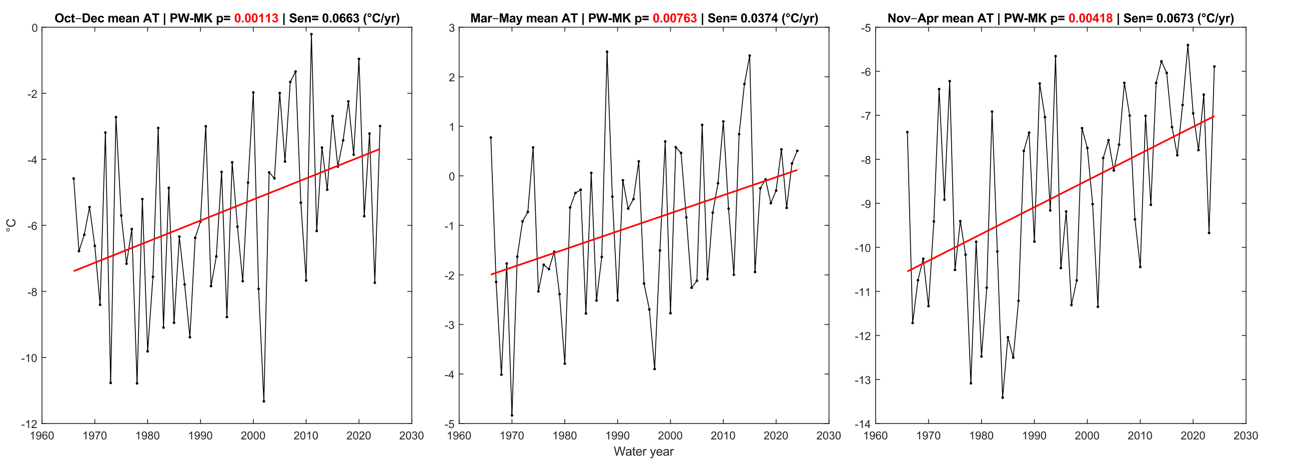

Figure 12 Long-term trends in seasonal air temperature (AT) (WY1966–WY2024; n=59).

FDD accumulated from WY start to CCT increased at +0.956 °C·days/yr (p=0.010). FDD accumulated from CCT to CWT decreased at −13.9 °C·days/yr (p<0.001), and full water-year FDD decreased at −12.5 °C·days/yr (p=0.002). TDD accumulated from WY start to CWT increased at +0.76 °C·days/yr (p=0.044) and full water-year TDD increased at +6.78 °C·days/yr (p=0.003). TDD accumulated from CCT to CWT showed no significant trend (Sen=−0.104 °C·days/yr, p=0.278) (Figure 13).

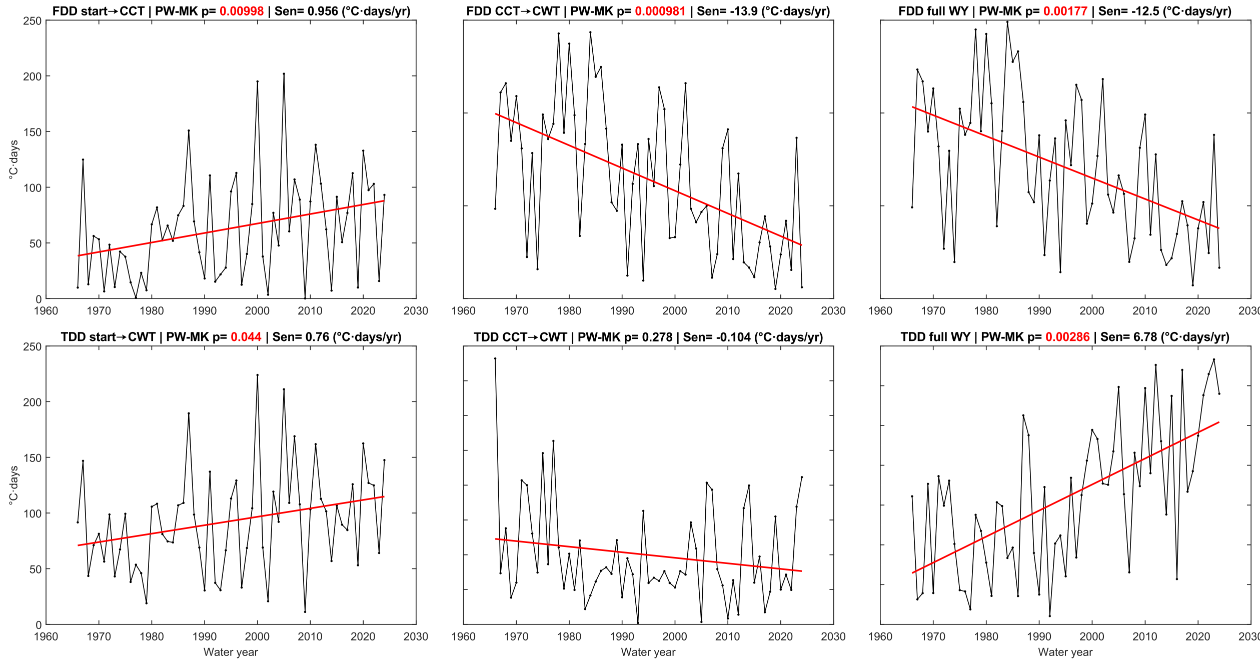

Figure 13 Long-term trends in freezing and thawing degree-day (FDD/TDD) linked to the ZCAT transition timings (WY1966–WY2024; n=59).

Annual maximum discharge (p=0.896), minimum discharge (p=0.172), and average discharge during the DSP (p=0.178) showed no significant trends. Maximum snow depth (p=0.539) and average snow depth during the CSP (p=0.295) showed no significant trends. Annual maximum air temperature (p=0.156) and average air temperature during the CDP (p=0.261) showed no significant trends. Annual minimum air temperature increased at +0.060 °C/yr (p=0.050), the only significant extreme metric (Figure 14).

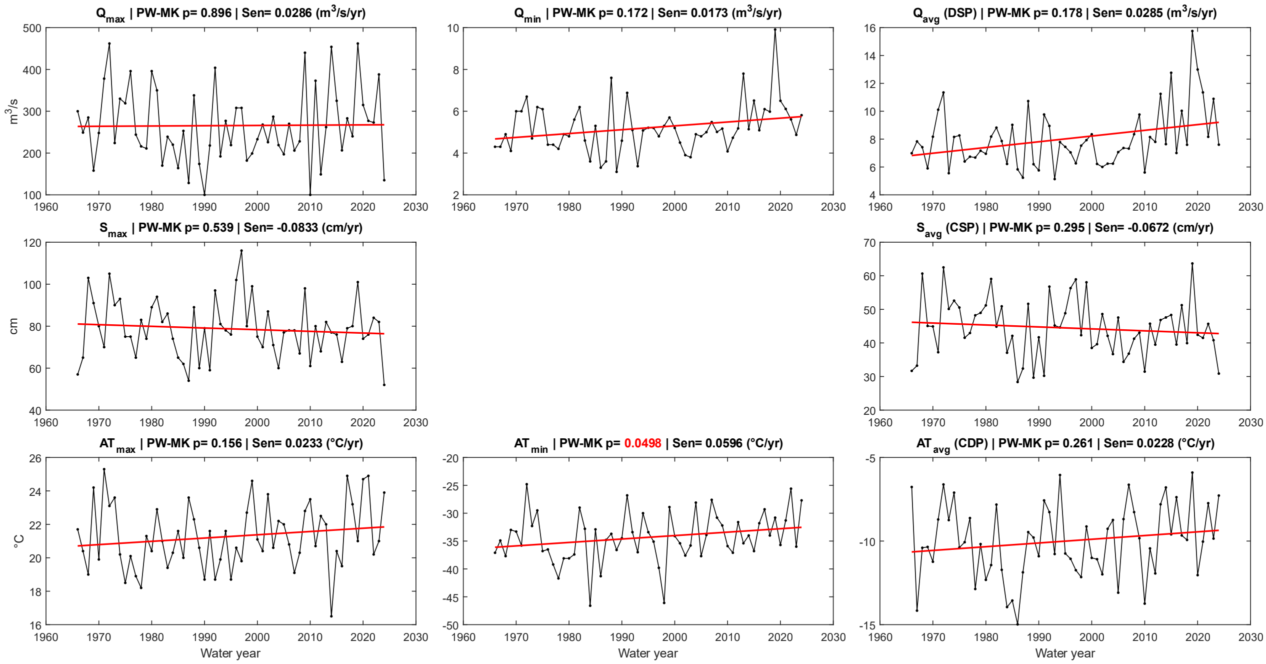

Figure 14 Long-term trends in hydroclimatic extreme-value and their average within IVIs (WY1966–WY2024; n=59).

4 Discussion

Our results form a coherent picture of asymmetric change in proxy-based transition timing at the River Oulankajoki over 59 WYs. Thermally-derived transitions (CCT, CWT) shifted faster and further than their surface response transitions (DSO, CSO, DSE, CSE), and this asymmetry was more coherent and systematic in the release-group, where all three PCTs shifted significantly but CWT shifted furthest, than in the onset-group, where only the thermally-derived CCT shifted significantly while surface proxies remained trendless. Among the onset group, the thermally-derived CCT shifted significantly (+0.538 d/yr, p=0.001), while the surface response proxies DSO and CSO showed no significant trend. At the period level, this contrast is stark: CCT shifted +17.5 d between the early and late sub-periods, compared with only +2.5 d for DSO and +4.0 d for CSO. In the release group, CWT shifted −12.5 d versus −3.0 d for DSE and −1.5 d for CSE. Air temperature is measured at a single point approximately 500 m from the gauge, while discharge integrates the entire upstream basin; this spatial mismatch can contribute to occasional ordering reversals in onset-group PCTs (e.g., DSO preceding CSO or CCT), particularly in years with early baseflow stabilization or delayed cumulative cooling. Figure S3 shows three example water years (WY1975, WY2011, and WY2020) in which these reversals occur. Among the release group, CWT, DSE, and CSE all shifted to earlier days, with CWT carrying the largest shift (−0.357 d/yr, p=0.002). These PCT shifts are consistent with the observed warming across all three seasonal windows: Oct–Dec mean AT increased at +0.066°C/yr (p=0.001), Nov–Apr at +0.067°C/yr (p=0.004), and Mar–May at +0.037°C/yr (p=0.008), indicating that both the onset and release seasons warmed significantly over the record.

This difference is consistent with release-group PCTs being more tightly governed by progressive atmospheric warming, whereas onset-group PCTs remained subject to localized and stochastic controls, such as precipitation phase, surface insulation, and early snowfall events. Prior studies report that river ice release timing across North America and Europe has advanced at approximately 0.6 days per decade, closely linked to warming temperatures (Chen and She, 2020; Newton and Mullan, 2021), while onset timing trends remain spatially heterogeneous and weakly correlated with climate signals (Liston and Hall, 1995; Prowse and Bonsal, 2004), which is consistent with the pattern observed at this case study site. The sequencing analysis reinforces this structure; within the onset-group, CCT, DSO, and CSO exhibited flexible interannual rankings, with five of six possible orderings occurring across the 59-year record. Moreover, the dominant ordering CSO→CCT→DSO increased in frequency from 37.9% in the early period to 46.7% in the late period, suggesting a gradual consolidation of onset-group sequencing consistent with CCT shifting progressively later relative to the surface proxies. In contrast, the release-group maintained the invariant ordering CWT→DSE→CSE in all 59 years. The correlation structure further supports this asymmetry; strong pairwise correlations among release-group PCTs (CWT and DSE: $r=0.60$; CWT and CSE: $r=0.53$; DSE and CSE: $r=0.74$) contrasted with weaker and more variable correlations among onset-group PCTs, particularly in the early period. In the late period, however, onset-group internal coupling strengthened, with CSO–CCT reaching $r=0.68$ and DSO–CCT $r=0.52$, both non-significant in the early period. Concurrently, release-group correlations weakened (DSE–CSE from $r=0.82$ to $r=0.60$), and DSO and DSE became significantly negatively correlated ($r=-0.45$, $p=0.013$), suggesting that earlier DSE is increasingly occurring in years with later DSO, a structural decoupling between onset and release in the discharge regime.

The CDP shortened at −0.871 d/yr ($p<0.001$), the largest IVI trend in the dataset, contracting simultaneously from both ends as CCT shifted later and CWT shifted earlier. FDD accumulated between CCT and CWT declined at −13.9 °C·days/yr ($p<0.001$), which indicates that the thermal winter narrowed in both duration and cold intensity. Notably, FDD accumulated from the WY start to CCT increased at +0.956 °C·days/yr ($p=0.010$), indicating that early-season cold accumulation intensified even as the overall cold period contracted. The CDP therefore narrowed primarily through a later onset of the cooling-dominant phase and an earlier end, rather than through a uniform reduction in cold intensity across the season. Full water-year FDD also declined (−12.5 °C·days/yr, $p=0.002$), while full water-year TDD increased (+6.78 °C·days/yr, $p=0.003$), which further supports the rebalancing of the annual thermal budget away from cold accumulation and toward warm accumulation driven primarily by the inward movement of CDP boundaries. DSP shortened significantly (−0.333 d/yr, $p=0.041$), which is consistent with DSE shifting earlier. CSP showed a negative Sen's slope but did not reach significance ($p=0.089$), consistent with the smaller period-level shift in CSE (−1.5 d) relative to CWT (−12.5 d) between sub-periods. These results at this site are directionally consistent with reported trends of earlier seasonal transitions across Arctic and sub-Arctic systems (Dauginis and Brown, 2021; Fukś, 2023; Markus et al., 2009; Newton and Mullan, 2021; Podkowa et al., 2023; Sharma et al., 2016; Wang and Feng, 2024), though generalization beyond this site is not made here.

We also identified two significant changes in CVIs, the temporal offsets between thermally-derived and surface response transitions. The interval between CSO and CCT increased at +0.333 d/yr (p=0.040), meaning CCT shifted later relative to CSO over the record. The interval between CSE and CWT shifted at −0.231 d/yr (p=0.011), which means CWT advanced faster than CSE. The interval between DSE and CWT shifted in the same direction but did not reach significance (p=0.102). The interval between DSE and CSE remained stationary (Sen=0.000 d/yr, p=0.958), both DSE and CSE shifted almost in parallel throughout the record. A number of studies report that despite earlier atmospheric warming, surface responses have lagged in sub-Arctic and boreal systems (Schwartz et al., 2006; Stone et al., 2002). This growing offset between thermally-derived and surface response transitions in systems with similar thermal-nival structure, poses challenges for hydrological modelling and ecosystem forecasting, as degree-day and temperature-threshold models may increasingly misestimate the timing of surface-driven responses (Bjorkman et al., 2015; Groisman and Easterling, 1994; Siegel et al., 2022). The smaller shift in CSE relative to CWT (−1.5 d vs −12.5 d) may also partly reflect that CSO/CSE are based on terrestrial snow depth at a single station rather than snow conditions on the river surface.

Despite significant shifts in PCT timing and IVI duration, all discharge and snow depth magnitude metrics remained statistically unchanged over the 59-year record. Neither maximum discharge (p=0.896) nor minimum discharge (p=0.172) showed a significant trend. Average discharge during the DSP showed no significant trend (p=0.178). Maximum snow depth (p=0.539) and average snow depth during the CSP (p=0.295) also remained stable. Annual minimum air temperature increased at +0.060 °C/yr (p=0.050), the only significant extreme metric, while annual maximum air temperature showed no significant trend (p=0.156). These findings align with studies reporting resilience in streamflow and snow depth magnitudes despite substantial hydroclimatic timing shifts (Harder et al., 2015; Shiklomanov et al., 2007), with increases in winter baseflow in northern basins attributed to permafrost thaw and deeper infiltration (St. Jacques and Sauchyn, 2009). Although some studies report increasing peak flows in certain regions (Burn et al., 2010; Byun et al., 2019), maximum discharge at this site remained stable over the record (p=0.896).

Changes in the timing of onset-group and release-group PCTs alter the seasonal windows available for sediment and nutrient transport, aquatic habitat structure, and biological processes. Earlier shifts in release-group PCTs and a contracting CDP affect the timing of ecological cues that depend on seasonal temperature and flow structure (Janowicz, 2010; Prowse et al., 2011). Shorter DSP periods affect the reliability of winter infrastructure dependent on stable low-flow periods in northern communities (Prowse et al., 2007).

All findings in this study are specific to the River Oulankajoki at the Oulanka gauging station over WY1966–WY2024. Winter discharge values in the source record are operationally corrected estimates (quality code 'Redukoitu'), meaning DSO and DSE are derived from a quality-controlled rather than a directly measured series and should be interpreted accordingly as discharge regime transition proxies. Additionally, the two discharge timings differ in their sensitivity to the DVD stability threshold. Replacing the SD-based threshold with an IQR-based alternative (IQR/1.349) shifts DSO by a median of 91 days but DSE by only 7 days. This has little bearing on our conclusions: DSE, which carries the significant earlier trend (p=0.023) and provides the statistically reliable component of the DSP shortening, is robust to the threshold choice, whereas the threshold-sensitive DSO shows no significant trend (p=0.281) and underpins no conclusion drawn here. The discharge-based findings are therefore not contingent on the SD-versus-IQR choice, although the absolute timing of DSO should be regarded as method-dependent. Independent observational context was provided by ice thickness measurement records (WY1980–WY1994, n=15) and water temperature winter gap data (WY1970–WY2024, n=55); however, both datasets are operationally constrained and neither constitutes a direct freeze-up or break-up observation, their temporal relationship with the proxy PCTs shows considerable interannual spread (Figure S2), and they should be interpreted as plausibility checks rather than validation. The proxy framework used here is most appropriate for unregulated boreal rivers without frequent mid-winter melt events; applicability to regulated or hydropeaking systems would require re-evaluation of the DVD stability definition.

5 Conclusions

This study provides a 59-year assessment of seasonal cryo-hydrological dynamics in a sub-Arctic river system using a structured detection approach across six key timing metrics. By applying the RiTiCE framework to the River Oulankajoki, we document a coherent and statistically significant shift in release-group timings including CSE, DSE, and CWT toward earlier dates, while onset-group PCTs (DSO, CSO) remain temporally unstable and trendless, CCT shifted significantly later. This divergence highlights a growing seasonal asymmetry in proxy-detected transition timing at this site. The analysis reveals that changes in phase transition timing are not occurring in isolation. CDP and DSP have shortened, while the offset between CSE and CWT widened. Lags between atmospheric transitions and surface responses have also evolved, release-group surface transitions are increasingly delayed relative to CWT, while onset-group transitions show no systematic delay relative to CCT. These trends document differential rates of shift between thermally-derived and surface response proxies, rather than a uniform seasonal shift.

Despite these structural changes, hydrological extremes such as peak discharge and maximum snow depth remain relatively stable. The results demonstrate that proxy-detected seasonal transitions at this site show increasing differential rates of shift under continued warming. The differential shifts between thermally-derived and surface proxy transitions pose a challenge for proxy-based forecasting of seasonal conditions, assessing flood risk, and managing aquatic ecosystems. These findings underscore the need for long-term observational records and improved process-based models that incorporate not only temperature thresholds but also lagged hydrological responses and transitional variability under continued warming at this site and in systems with similar thermal-nival structure.

Appendices

Appendix A

https://figshare.com/s/d6dc8875fd8151a80085

Data availability

All data supporting the findings of this study are publicly available at:
FMI Open Data Portal: https://en.ilmatieteenlaitos.fi/open-data
Finnish Environmental Institute (SYKE): https://wwwp2.ymparisto.fi/scripts/kirjaudu.asp

Author contribution

A.J.S. conceived the study, developed the methodology, processed and analyzed the data, wrote the manuscript, and prepared all figures. A.A. contributed to the interpretation of results and manuscript preparation. A.T.H. supervised the study.

Competing interests

The authors declare that they have no conflict of interest.

Acknowledgements

The authors gratefully acknowledge the Maa- ja vesitekniikan tuki ry (MVTT) for funding this research through grant no. 4802. We thank the Oulanka Research Station for long-term hydrological monitoring and infrastructure support. We are also grateful to SYKE (Finnish Environment Institute) and the Finnish Meteorological Institute (FMI) for providing the datasets. We appreciate the efforts of all personnel involved in field measurements and data collection over this 59-year record. Artificial intelligence tools were used in a limited capacity to assist with code refinement, code commenting, instruction generation, and language editing of the manuscript. No scientific concepts, methodology, or analytical logic were generated by AI.

References

Arvola, L. and Nurmesniemi, A.: Seasonal dynamics of plankton in two boreal rivers in northern Finland, SIL Proceedings, 1922-2010, 27, 1928–1932, https://doi.org/10.1080/03680770.1998.11901578, 2000.

Bennett, K. E. and Prowse, T. D.: Northern Hemisphere geography of ice-covered rivers, Hydrological Processes, 24, 235–240, https://doi.org/10.1002/hyp.7561, 2010.

Bieniek, P. A., Bhatt, U. S., Rundquist, L. A., Lindsey, S. D., Zhang, X., and Thoman, R. L.: Large-scale climate controls of interior Alaska river ice breakup, Journal of Climate, 24, 286–297, 2011.

Bjorkman, A. D., Elmendorf, S. C., Beamish, A. L., Vellend, M., and Henry, G. H. R.: Contrasting effects of warming and increased snowfall on Arctic tundra plant phenology over the past two decades, Global Change Biology, 21, 4651–4661, https://doi.org/10.1111/gcb.13051, 2015.

Blåfield, L., Marttila, H., Kasvi, E., and Alho, P.: Temporal shift of hydroclimatic regime and its influence on migration of a high latitude meandering river, Journal of Hydrology, 633, 130935, 2024.

Box, J. E., Colgan, W. T., Christensen, T. R., Schmidt, N. M., Lund, M., Parmentier, F.-J. W., Brown, R., Bhatt, U. S., Euskirchen, E. S., and Romanovsky, V. E.: Key indicators of Arctic climate change: 1971–2017, Environmental Research Letters, 14, 045010, 2019.

Bring, A., Fedorova, I., Dibike, Y., Hinzman, L., Mård, J., Mernild, S. H., Prowse, T., Semenova, O., Stuefer, S. L., and Woo, M.-K.: Arctic terrestrial hydrology: A synthesis of processes, regional effects, and research challenges, Journal of Geophysical Research: Biogeosciences, 121, 621–649, 2016.

Brown, D. R., Brinkman, T. J., Verbyla, D. L., Brown, C. L., Cold, H. S., and Hollingsworth, T. N.: Changing river ice seasonality and impacts on interior Alaskan communities, Weather, Climate, and Society, 10, 625–640, 2018.

Burn, D. H., Sharif, M., and Zhang, K.: Detection of trends in hydrological extremes for Canadian watersheds, Hydrological Processes, 24, 1781–1790, https://doi.org/10.1002/hyp.7625, 2010.

Burrell, B. C., Beltaos, S., and Turcotte, B.: Effects of climate change on river-ice processes and ice jams, International Journal of River Basin Management, 21, 421–441, https://doi.org/10.1080/15715124.2021.2007936, 2023.

Byun, K., Chiu, C.-M., and Hamlet, A. F.: Effects of 21st century climate change on seasonal flow regimes and hydrologic extremes over the Midwest and Great Lakes region of the US, Science of the Total Environment, 650, 1261–1277, 2019.

Chen, Y. and She, Y.: Long-term variations of river ice breakup timing across Canada and its response to climate change, Cold Regions Science and Technology, 176, 103091, 2020.

Dauginis, A. A. and Brown, L. C.: Recent changes in pan-Arctic sea ice, lake ice, and snow-on/off timing, The Cryosphere, 15, 4781–4805, 2021.

Feng, D., Gleason, C. J., Lin, P., Yang, X., Pan, M., and Ishitsuka, Y.: Recent changes to Arctic river discharge, Nature communications, 12, 6917, 2021.

Finnish Meteorological Institute: Daily Air Temperature and Snow Depth Observations, Kuusamo Kiutaköngäs Weather Station, 2026.

Fukś, M.: Changes in river ice cover in the context of climate change and dam impacts: a review, Aquat Sci, 85, 113, https://doi.org/10.1007/s00027-023-01011-4, 2023.

García Criado, M., Myers-Smith, I. H., Bjorkman, A. D., Elmendorf, S. C., Normand, S., Aastrup, P., Aerts, R., Alatalo, J. M., Baeten, L., and Björk, R. G.: Plant diversity dynamics over space and time in a warming Arctic, Nature, 1–9, 2025.

Groisman, P. Y. and Easterling, D. R.: Variability and trends of total precipitation and snowfall over the United States and Canada, Journal of Climate, 7, 184–205, 1994.

Harder, P., Pomeroy, J. W., and Westbrook, C. J.: Hydrological resilience of a Canadian Rockies headwaters basin subject to changing climate, extreme weather, and forest management, Hydrological Processes, 29, 3905–3924, https://doi.org/10.1002/hyp.10596, 2015.

IAHR: International Association for Hydraulic Research Association, MULTILINGUAL ICE TERMINOLOGY, 1980.

Ionita, M., Badaluta, C.-A., Scholz, P., and Chelcea, S.: Vanishing river ice cover in the lower part of the Danube basin–signs of a changing climate, Scientific Reports, 8, 7948, 2018.

Jalali Shahrood, A.: Past, present, and future of river flow regime in Nordic region focusing on river ice break-up events, 2023.

Jalali Shahrood, A., Ahrari, A., Rossi, P. M., Klöve, B., and Torabi Haghighi, A.: RiTiCE: River Flow Timing Characteristics and Extremes in the Arctic Region, Water, 15, 861, 2023.

Jalali Shahrood, A., Ahrari, A., Karjalainen, N., Klöve, B., and Haghighi, A. T.: Application of RiTiCE in understanding hydro-meteorological controls on ice break-up patterns in River Tornionjoki, Environ Monit Assess, 196, 764, https://doi.org/10.1007/s10661-024-12910-w, 2024.

Janowicz, J. R.: Observed trends in the river ice regimes of northwest Canada, Hydrology Research, 41, 462–470, 2010.

Kendall, M. G.: Rank correlation methods, 4th ed., Charles Griffin, London, 202 pp., 1975.

Lehnherr, I., St. Louis, V. L., Sharp, M., Gardner, A. S., Smol, J. P., Schiff, S. L., Muir, D. C., Mortimer, C. A., Michelutti, N., and Tarnocai, C.: The world's largest High Arctic lake responds rapidly to climate warming, Nature communications, 9, 1290, 2018.

Lesack, L. F., Marsh, P., Hicks, F. E., and Forbes, D. L.: Local spring warming drives earlier river-ice breakup in a large Arctic delta, Geophysical Research Letters, 41, 1560–1567, 2014.

Liljedahl, A. K., Boike, J., Daanen, R. P., Fedorov, A. N., Frost, G. V., Grosse, G., Hinzman, L. D., Iijma, Y., Jorgenson, J. C., and Matveyeva, N.: Pan-Arctic ice-wedge degradation in warming permafrost and its influence on tundra hydrology, Nature geoscience, 9, 312–318, 2016.

Liston, G. E. and Hall, D. K.: Sensitivity of lake freeze-up and break-up to climate change: a physically based modeling study, Annals of Glaciology, 21, 387–393, 1995.

Magnuson, J. J., Robertson, D. M., Benson, B. J., Wynne, R. H., Livingstone, D. M., Arai, T., Assel, R. A., Barry, R. G., Card, V., and Kuusisto, E.: Historical trends in lake and river ice cover in the Northern Hemisphere, Science, 289, 1743–1746, 2000.

Mann, H. B.: Nonparametric tests against trend, Econometrica: Journal of the econometric society, 245–259, 1945.

Markus, T., Stroeve, J. C., and Miller, J.: Recent changes in Arctic sea ice melt onset, freezeup, and melt season length, J. Geophys. Res., 114, 2009JC005436, https://doi.org/10.1029/2009JC005436, 2009.

Masson-Delmotte, V., Zhai, P., Pirani, A., Connors, S. L., Péan, C., Berger, S., Caud, N., Chen, Y., Goldfarb, L., and Gomis, M. I.: Climate change 2021: the physical science basis, Contribution of working group I to the sixth assessment report of the intergovernmental panel on climate change, 2, 2391, 2021.

Nalbant, M. A. and Sharma, S.: Investigating the impact of climate change on river ice thickness across the Northern Belt of United States, ISH Journal of Hydraulic Engineering, 29, 217–231, https://doi.org/10.1080/09715010.2022.2050309, 2023.

Newton, A. M. and Mullan, D. J.: Climate change and Northern Hemisphere lake and river ice phenology from 1931–2005, The Cryosphere, 15, 2211–2234, 2021.

Park, H., Yoshikawa, Y., Oshima, K., Kim, Y., Ngo-Duc, T., Kimball, J. S., and Yang, D.: Quantification of warming climate-induced changes in terrestrial Arctic river ice thickness and phenology, Journal of Climate, 29, 1733–1754, 2016.

Pavelsky, T. M. and Zarnetske, J. P.: Rapid decline in river icings detected in Arctic Alaska: Implications for a changing hydrologic cycle and river ecosystems, Geophysical Research Letters, 44, 3228–3235, https://doi.org/10.1002/2016GL072397, 2017.

Podkowa, A., Kugler, Z., Nghiem, S. V., and Brakenridge, G. R.: Ice Freeze-Up and Break-Up in Arctic Rivers Observed With Satellite L-Band Passive Microwave Data From 2010 to 2020, Water Resources Research, 59, e2022WR031939, https://doi.org/10.1029/2022WR031939, 2023.

Prowse, T., Alfredsen, K., Beltaos, S., Bonsal, B. R., Bowden, W. B., Duguay, C. R., Korhola, A., McNamara, J., Vincent, W. F., Vuglinsky, V., Walter Anthony, K. M., and Weyhenmeyer, G. A.: Effects of Changes in Arctic Lake and River Ice, AMBIO, 40, 63–74, https://doi.org/10.1007/s13280-011-0217-6, 2011.

Prowse, T. D. and Bonsal, B. R.: Historical trends in river-ice break-up: a review, Hydrology Research, 35, 281–293, 2004.

Prowse, T. D., Wrona, F. J., Reist, J. D., Gibson, J. J., Hobbie, J. E., Lévesque, L. M., and Vincent, W. F.: Climate change effects on hydroecology of Arctic freshwater ecosystems, AMBIO: A Journal of the Human Environment, 35, 347–358, 2006.

Prowse, T. D., Bonsal, B. R., Duguay, C. R., and Lacroix, M. P.: River-ice break-up/freeze-up: a review of climatic drivers, historical trends and future predictions, Annals of Glaciology, 46, 443–451, 2007.

Rokaya, P., Morales-Marín, L., Bonsal, B., Wheater, H., and Lindenschmidt, K.-E.: Climatic effects on ice phenology and ice-jam flooding of the Athabasca River in western Canada, Hydrological Sciences Journal, 64, 1265–1278, https://doi.org/10.1080/02626667.2019.1638927, 2019.

Saraniemi, M., Huusko, A., and Tahkola, H.: Spawning migration and habitat use of adfluvial brown trout, Salmo trutta, in a strongly seasonal boreal river., Boreal environment research, 13, 2008.

Schwartz, M. D., Ahas, R., and Aasa, A.: Onset of spring starting earlier across the Northern Hemisphere, Global Change Biology, 12, 343–351, https://doi.org/10.1111/j.1365-2486.2005.01097.x, 2006.

Sen, P. K.: Estimates of the regression coefficient based on Kendall's tau, Journal of the American statistical association, 63, 1379–1389, 1968.

Sharma, S., Magnuson, J. J., Batt, R. D., Winslow, L. A., Korhonen, J., and Aono, Y.: Direct observations of ice seasonality reveal changes in climate over the past 320–570 years, Sci Rep, 6, 25061, https://doi.org/10.1038/srep25061, 2016.

Sharma, S., Filazzola, A., Nguyen, T., Imrit, M. A., Blagrave, K., Bouffard, D., Daly, J., Feldman, H., Feldsine, N., and Hendricks-Franssen, H.-J.: Long-term ice phenology records spanning up to 578 years for 78 lakes around the Northern Hemisphere, Scientific Data, 9, 318, 2022.

Shen, H. T.: River Ice Processes, in: Advances in Water Resources Management, edited by: Wang, L. K., Yang, C. T., and Wang, M.-H. S., Springer International Publishing, Cham, 483–530, https://doi.org/10.1007/978-3-319-22924-9_9, 2016.

Shiklomanov, A. I. and Lammers, R. B.: River ice responses to a warming Arctic—recent evidence from Russian rivers, Environmental Research Letters, 9, 035008, 2014.

Shiklomanov, A. I., Lammers, R. B., Rawlins, M. A., Smith, L. C., and Pavelsky, T. M.: Temporal and spatial variations in maximum river discharge from a new Russian data set, Journal of geophysical research: Biogeosciences, 112, 2007.

Siegel, J. E., Fullerton, A. H., and Jordan, C. E.: Accounting for snowpack and time-varying lags in statistical models of stream temperature, Journal of Hydrology X, 17, 100136, 2022.

Spearman, C.: The Proof and Measurement of Association between Two Things, The American Journal of Psychology, 15, 72, https://doi.org/10.2307/1412159, 1904.

St. Jacques, J.-M. and Sauchyn, D. J.: Increasing winter baseflow and mean annual streamflow from possible permafrost thawing in the Northwest Territories, Canada, Geophysical Research Letters, 36, 2009.

Stone, R. S., Dutton, E. G., Harris, J. M., and Longenecker, D.: Earlier spring snowmelt in northern Alaska as an indicator of climate change, J. Geophys. Res., 107, https://doi.org/10.1029/2000JD000286, 2002.

SYKE: Daily River Discharge Measurements, Oulanka Research Station, 2026.

Takács, K. and Kern, Z.: Multidecadal changes in the river ice regime of the lower course of the River Drava since AD 1875, Journal of Hydrology, 529, 1890–1900, 2015.

Von Storch, H.: Misuses of Statistical Analysis in Climate Research, in: Analysis of Climate Variability, edited by: Von Storch, H. and Navarra, A., Springer Berlin Heidelberg, Berlin, Heidelberg, 11–26, https://doi.org/10.1007/978-3-662-03744-7_2, 1999.

Vuglinsky, V.: Assessment of changes in ice regime characteristics of Russian lakes and rivers under current climate conditions, Natural Resources, 8, 416, 2017.

Vuglinsky, V. and Valatin, D.: Changes in ice cover duration and maximum ice thickness for rivers and lakes in the Asian part of Russia, Natural Resources, 9, 73, 2018.

Wang, X. and Feng, L.: Patterns and Trends in Northern Hemisphere River Ice Phenology from 2000 to 2021, Remote Sensing of Environment, 313, 114346, https://doi.org/10.1016/j.rse.2024.114346, 2024.

Yang, X., Pavelsky, T. M., and Allen, G. H.: The past and future of global river ice, Nature, 577, 69–73, 2020.